Proceedings of Equadiff-11
2005, pp. 213–222
ISBN 978-80-227-2624-5

ARBITRARY LAGRANGIAN EULERIAN METHOD FOR COMPRESSIBLE PLASMA SIMULATIONS*

RICHARD LISKA† AND MILAN KUCHAŘÍK‡

Abstract. Laser plasma is modeled by Lagrangian hydrodynamical equations including heat conductivity and laser absorption. The hyperbolic part of the model is treated by Arbitrary Lagrangian Eulerian (ALE) method which avoids moving mesh distortion and parabolic heat conductivity part is treated by splitting and mimetic method. High velocity laser accelerated disc impact problems for which standard Lagrangian simulation method fails are treated well by the ALE method.

Key words. Euler equations, Lagrangian hydrodynamics, ALE, laser plasma simulations

AMS subject classifications. 35L60, 35L65, 76N1

1. Introduction. Compressible laser plasma typically includes regions of high compression and/or large expansion which require treatment by Lagrangian hydrodynamics allowing large scale changes of computational domain with moving boundaries and moving boundary conditions. The Euler equations for compressible fluid in Lagrangian coordinates with heat conductivity and laser absorption are

$$\frac{\mathrm{d}\,\rho}{\mathrm{d}\,t} + \rho \,\mathrm{div}\,\mathbf{u} = 0, \qquad \frac{\mathrm{d}\,\mathbf{x}}{\mathrm{d}\,t} = \mathbf{u} \tag{1.1}$$

$$\rho \frac{\mathrm{d}\,\mathbf{u}}{\mathrm{d}\,t} + \mathrm{grad}\ p = 0 \tag{1.2}$$

$$\rho \frac{\mathrm{d}\,\epsilon}{\mathrm{d}\,t} + p \,\mathrm{div}\,\mathbf{u} = \mathrm{div}(\kappa \,\mathrm{grad}\ T) - \mathrm{div}(I) \tag{1.3}$$

where $\mathbf{x}$ is position, t time, ρ density, $\mathbf{u}$ fluid velocity, p pressure, $\epsilon = E/\rho - \mathbf{u}^2/2$ specific internal energy, E density of total energy, T temperature κ heat conductivity coefficient and I laser intensity. The total Lagrangian time derivatives include convective terms

$$\frac{\mathrm{d}}{\mathrm{d}\,t} = \frac{\partial}{\partial\, t} + \mathbf{u} \cdot \mathrm{grad}\,.$$

The computational mesh is fixed to the fluid and moves with the fluid. Its movement is described by the second equation from (1.1) which is ordinary differential equation being solved for every node of the mesh. As the mesh is moving with the fluid there is no mass flux between cells through the mesh edges.

In some cases (e.g. in problems involving shear flows) however the moving mesh can degenerate and become invalid with inverted cells when some node crosses the opposite edge of the same cell. An example of such problem is presented in FIG. 1.1. The FIG. 1.1(a) presents the initial conditions, the lighter part on left has higher density and is at rest, while the darker part on right has lower density and is moving by high velocity to the

*This work was supported in part by the Czech Ministry of Education grant MSM 6840770022.

† Czech Technical University in Prague, Faculty of Nuclear Sciences and Physical Engineering, Břehová 7, 115 19 Prague 1, Czech Republic, liska@siduri.fjfi.cvut.cz

‡ Los Alamos National Laboratory, T-7, MS B284, Los Alamos, NM 87545, U.S.A. kucharik@lanl.gov

left. The results for this disc impact problem computed by pure Lagrangian method is presented in FIG. 1.1(b), the mesh is severely distorted and will soon become invalid so that the Lagrangian computation cannot continue.

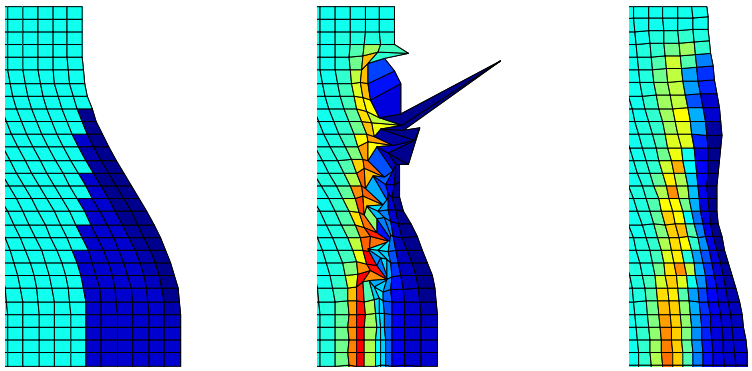

FIG. 1.1. *Density profiles of homogeneous disc impact problem: (a) Initial conditions, (b) Results of pure Lagrangian simulation, (c) Results of ALE simulation.*

The mesh distortion can be avoided by using Arbitrary Lagrangian Eulerian (ALE) method [11] as shown for the same problem in FIG. 1.1(c). The ALE method is a combination of Lagrangian and Eulerian methods and consists of three phases. In the first phase several time steps of standard Lagrangian computation are performed. The second phase is rezoning which smooths the distorted computational mesh. And the last third phase is remapping which conservatively interpolate (remaps) the conservative quantities from the old to the new, better mesh. After remapping the method returns to the Lagrangian computation in the first phase. Remapping corresponds to the Eulerian part of ALE method and allows mass flux between cells. ALE method combines positives of both approaches, the mesh moves with fluid (as Lagrangian), but Eulerian part keeps the mesh smooth.

The ALE method is recently becoming more and more popular [16, 1, 3, 15].

2. Lagrangian Hydrodynamics. The hyperbolic part of our system (1.1)–(1.3) (omitting heat conductivity and laser absorption) is standard Lagrangian hydrodynamics and is numerically treated by compatible method [7, 5]. Scalar quantities (density, pressure, internal energy, temperature) are defined inside grid cells, vector quantities (positions, velocities) are defined at grid nodes. We use logically rectangular quadrilateral mesh.

Compatible hydrodynamics method is based on zonal, subzonal, and viscosity forces acting on each grid node. The zonal pressure force is the force from all neighboring grid cells to the node due to the pressure inside cells. The subzonal pressure force [8] depends on the difference between the pressure in cell, and the pressure in cell corners (the cell corner is a quadrilateral whose vertexes are one node, one center of a cell and two centers of edges). The subzonal pressure force reduces artificial hourglass type grid distortions and is controlled by merit factor. Viscosity force adds artificial viscosity which is the essential part of the compatible method. The simplest bulk viscosity is based on Kuropatenko formula [14]. Other possibilities include more complicated edge viscosity [6] or tensor viscosity [4]. One can include other force sources as gravity or laser absorption

in the Lagrangian hydrodynamics.

3. Rezoning. The rezoning phase of the ALE method covers mesh smoothing and untangling. For remapping we need to move only those vertexes which are necessary to move and as little as possible. There exist several methods for rezoning, e.g. combination of feasible set method and numerical optimization [20] or reference Jacobian method [12].

One of the simplest methods which we use is Winslow smoothing method [21]. The new positions of the mesh nodes are computed (with possible iteration over l starting at old Lagrangian mesh) as

$$\vec{x}_{i,j}^{\,l+1} = \frac{1}{2\,(\alpha^l + \gamma^l)} \Big(\alpha^l\,(\vec{x}_{i,j+1}^{\,l} + \vec{x}_{i,j-1}^{\,l}) + \gamma^l\,(\vec{x}_{i+1,j}^{\,l} + \vec{x}_{i-1,j}^{\,l}) - \frac{1}{2}\,\beta^l\,(\vec{x}_{i+1,j+1}^{\,l} - \vec{x}_{i-1,j+1}^{\,l} + \vec{x}_{i-1,j-1}^{\,l} - \vec{x}_{i+1,j-1}^{\,l}) \Big),$$

where the coefficients $\alpha^l = x_\xi^2 + y_\xi^2$, $\beta^l = x_\xi\,x_\eta + y_\xi\,y_\eta$, $\gamma^l = x_\eta^2 + y_\eta^2$, and (ξ, η) are logical coordinates $\xi_i = i/M$, $\eta_j = j/N$ for $i = 0, \ldots, M$ and $j = 0, \ldots, N$. The derivatives x_ξ, x_η are approximated by the central differences

$$(x_\xi)_{i,j} \approx \frac{x_{i+1,j} - x_{i-1,j}}{2}\,, \qquad (x_\eta)_{i,j} \approx \frac{x_{i,j+1} - x_{i,j-1}}{2} \tag{3.1}$$

and similarly for y.

4. Remapping. The remapping phase of the ALE method is in fact conservative interpolation of conserved quantities from the old mesh to the new smoother one. We first perform piecewise linear reconstruction of conserved quantities (as density) on each cell of the old mesh with Barth-Jasperson limiter [2]. The reconstruction is followed by integration of reconstruction on the old mesh over cells of the new mesh to get total values (as mass) inside each new cell which together with cell volume results in new remapped value of conserved quantity on the new mesh. The most natural is the exact integration of reconstructed function over overlapped areas of new and old cells which however requires computing cells intersections which is rather slow. We use more effective approximate integration [13, 9] over regions swept by edges as the edges move from old mesh to the new one, see FIG. 4.1. The integral over new cell can be decomposed as sum of signed integrals over four swept regions and integral over the old cell. The volume integrals of reconstructed function are reduced to boundary integrals and evaluated exactly as reconstructed function is linear. So the new mass is

$$\tilde{m}^*_{i+\frac12,j+\frac12} = m_{i+\frac12,j+\frac12} + \mathcal{F}^*_{i+1,j+\frac12} + \mathcal{F}^*_{i,j+\frac12} + \mathcal{F}^*_{i+\frac12,j+1} + \mathcal{F}^*_{i+\frac12,j}\,,$$

where the mass of the swept region $\delta F_{i,j+\frac12}$ (quadrilateral $P_{i,j}, P_{i,j+1}, \tilde{P}_{i,j+1}, \tilde{P}_{i,j}$) is

$$\mathcal{F}^*_{i,j+\frac12} = \int\limits_{\delta F_{i,j+\frac12}} g_{i,j+\frac12}(x,y)\ \mathrm{d}V,$$

and reconstruction $g_{i,j+\frac12}(x,y)$ is taken from the appropriate cell (in which most of the swept region lies), e.g. in FIG. 4.1 it would be taken from cell $i - \frac12, j + \frac12$. The masses and volumes of swept regions are signed, e.g. all swept regions of the cell $i + \frac12, j + \frac12$ in FIG. 4.1 are positive as all four edges move in the outward direction. The described remapping method preserves linear functions.

However even with limiter reconstruction the remapping can introduce new extrema, i.e. it is not preserving local bounds. To preserve local bounds conservative redistribution, or repair [13, 18], redistributes mass to the neighboring cells so that the local bounds are preserved.

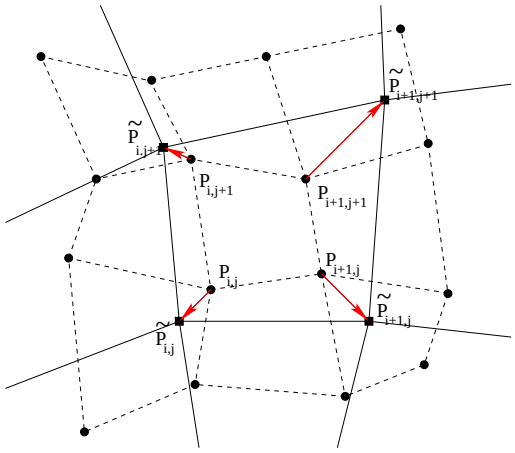

FIG. 4.1. *Old mesh with nodes $P_{i,j}$ and dashed edges, new mesh with nodes $\tilde{P}_{i,j}$ and solid line edges. One swept region is e.g. quadrilateral $P_{i,j}, P_{i,j+1}, \tilde{P}_{i,j+1}, \tilde{P}_{i,j}$ defined by the edge $P_{i,j}, P_{i,j+1}$ moving from the old to the new position.*

5. Heat conductivity. The parabolic part of energy equation (1.3)

$$\rho \frac{\partial \epsilon}{\partial t} = \operatorname{div}(\kappa \operatorname{grad} T)$$

is treated separately by splitting (on temporally static mesh) from hyperbolic part of the whole system (1.1)–(1.3). It is transformed to heat equation for temperature T

$$\rho \frac{\partial \epsilon}{\partial T} \frac{\partial T}{\partial t} = \operatorname{div}(\kappa \operatorname{grad} T).$$

For heat conductivity we use classical Spitzer-Harm plasma heat conductivity [19]

$$\kappa = C_\kappa \frac{T^{5/2}}{Z \ln \Lambda}$$

where T is temperature, Z ionization and $\ln \Lambda$ Coulomb logarithm. As the heat conductivity coefficient κ is non-linear function of temperature we can expect non-linear heat conductivity effects like heat waves, and the employed numerical method has to be able to deal with such effects.

We treat the space discretization of heat equation by the mimetic method [17] which we describe here on the elliptic Poisson equation

$$\begin{aligned} -\operatorname{div} \kappa \operatorname{grad} T &= f \qquad \text{on } V \\ (\kappa \operatorname{grad} T, \mathbf{n}) &= \psi \qquad \text{on } \partial V \end{aligned}$$

treated on region V with boundary ∂V with Neumann boundary conditions. The Poisson equation is transformed into the first order equations, so called flux form

$$\begin{aligned} \operatorname{div} \mathbf{w} &= f \\ \mathbf{w} &= -\kappa \operatorname{grad} T. \end{aligned}$$

We introduce the operators of generalized gradient

$$\mathbf{G}T = -\kappa \text{ grad } T$$

and extended divergence

$$\mathbf{D}\,\mathbf{w} = \begin{cases} \operatorname{div}\mathbf{w} & \text{on } V \\ -(\mathbf{w},\mathbf{n}) & \text{on } \partial V \end{cases} .$$

The integral properties of these operators are given by divergence Green formula and Gauss theorem. The divergence Green formula

$$\int_V \operatorname{div}\mathbf{w}\ \mathrm{d}V - \oint_{\partial V} (\mathbf{w},\mathbf{n})\ \mathrm{d}S = 0 \tag{5.1}$$

can be restated as $(\mathbf{D}\ \mathbf{w}, 1)_H = 0$ where we use the inner product on space H of scalar functions $(u,v)_H = \int_V u\ v\ \mathrm{d}V + \oint_{\partial V} u\ v\ \mathrm{d}S$. Gauss theorem

$$\int_V T \operatorname{div}\mathbf{w}\ \mathrm{d}V - \oint T(\mathbf{w},\mathbf{n})\ \mathrm{d}S + \int_V (\mathbf{w}, \kappa^{-1}\kappa \operatorname{grad} T)\,\mathrm{d}V = 0$$

can be restated as $(\mathbf{D}\mathbf{w}, T)_H = (\mathbf{w}, \mathbf{G}T)_{\mathbf{H}}$ where we use also the inner product on space $\mathbf{H}$ of vector functions $(\mathbf{A},\mathbf{B})_{\mathbf{H}} = \int_V (\kappa^{-1}\mathbf{A},\mathbf{B})\,\mathrm{d}V$. The operators $\mathbf{G},\mathbf{D}$ act between spaces $H,\mathbf{H}$ as $\mathbf{G}: H \to \mathbf{H}, \mathbf{D}: \mathbf{H} \to H$. Gauss theorem states that generalized gradient is adjoint operator of extended divergence $\mathbf{G} = \mathbf{D}^*$. The basic idea of support operator mimetic method [17] is to mimic these two integral properties also in discrete case on spaces of discrete functions.

We discretize a scalar function u by values U_{ij} inside each cell ij and U_k at the center of each boundary edge k and a vector flux function $\mathbf{w}$ at the center of each edge by the projections $W\xi_{i,j}, W\eta_{i,j}$ normal to the edge as shown in FIG. 5.1. This discretization of vector heat flux guarantees the continuity of normal flux through each edge. With these

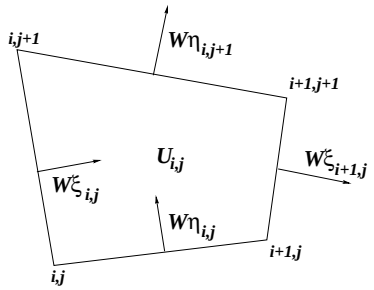

FIG. 5.1. *Scalar quantities U_{ij} are defined inside the cell and vector quantities $\mathbf{W}$ by projection of vector on edge normal at center of edges.*

discretizations we define the discrete function spaces $HC, \mathbf{HL}$ of scalar and vector grid functions respectively. On these discrete function spaces we define natural inner products as approximations of inner products on continuum function spaces. The natural inner product of scalar grid functions is

$$(U,V)_{HC} = \sum_{ij\in\overline{V}} U_{ij}\ V_{ij}\ VC_{ij} + \sum_{k\in\overline{\partial V}} U_k\ V_k\ S_k$$

where VC_{ij} is the volume of the cell ij, S_k is the length of the boundary edge k, $\overline{V}$ is set of all mesh cells and $\overline{\partial V}$ is set of boundary mesh edges. The natural inner product of vector grid functions is

$$(\mathbf{A},\mathbf{B})_{\mathbf{HL}} = \sum_{ij\in\overline{V}} (\mathbf{A},\mathbf{B})_{ij} \frac{VC_{ij}}{\kappa_{ij}}$$

where at cell ij we have

$$(\mathbf{A},\mathbf{B})_{ij} = \frac{1}{VC_{ij}} \sum_{k=0}^{1}\sum_{l=0}^{1} (\mathbf{A},\mathbf{B})_{ij}^{kl} V_{ij}^{kl}$$

and at the node ij of cell ij, i.e. $k=0$, $l=0$

$$(\mathbf{A},\mathbf{B})_{ij}^{00} = \frac{A\xi_{ij}B\xi_{ij} + A\eta_{ij}B\eta_{ij} + (A\xi_{ij}B\eta_{ij} + A\eta_{ij}B\xi_{ij})\cos\phi_{ij}^{00}}{\sin^2\phi_{ij}^{00}}$$

and the weights $V_{ij}^{kl} = VC_{ij}/4$ are used. To be able to evaluate the adjoint operator in natural inner products on discrete function spaces we also define formal inner products on discrete function spaces. The formal inner product of scalar grid functions is given by

$$[U,V]_{HC} = \sum_{ij\in\overline{V}} U_{ij}V_{ij} + \sum_{k\in\overline{\partial V}} U_k V_k,$$

and the formal inner product of vector grid functions by

$$[\mathbf{A},\mathbf{B}]_{\mathbf{HL}} = \sum_{ij\in\overline{V}} A\xi_{ij}B\xi_{ij} + A\eta_{ij}B\eta_{ij}.$$

The operators M, L connecting natural and formal inner products are defined by $(U,V)_{HC} = [MU,V]_{HC}$ and by $(\mathbf{A},\mathbf{B})_{\mathbf{HL}} = [L\mathbf{A},\mathbf{B}]_{\mathbf{HL}}$.

Divergence discretization is simply derived by applying the divergence Green formula (5.1) to one cell ij

$$(D\mathbf{W})_{ij} = \frac{1}{VC_{ij}}(W\xi_{i+1,j}S\xi_{i+1,j} - W\xi_{ij}S\xi_{ij} + W\eta_{i,j+1}S\eta_{i,j+1} - W\eta_{ij}S\eta_{ij}.)$$

On the boundary edge the extended divergence is given by $(D\mathbf{W})_{i0} = -W\eta_{i1}$, $(D\mathbf{W})_{iJ} = W\eta_{iJ}$, $(D\mathbf{W})_{0j} = -W\xi_{1j}$, $(D\mathbf{W})_{Ij} = W\xi_{Ij}$. Now the discrete generalized gradient is defined as adjoint of extended divergence in natural inner products $G = D^*$ so that $(D\mathbf{W},T)_{HC} = (\mathbf{W},D^*T)_{\mathbf{HL}}$. When we transform this into formal inner products we obtain $[\mathbf{W},D^{\otimes}MT]_{\mathbf{HL}} = [\mathbf{W},LD^*T]_{\mathbf{HL}}$ from which follows that $LD^* = D^{\otimes}M$ where the formal adjoint operator $D^{\otimes}$ can be constructed. So to get the gradient $\mathbf{W} = GT$ of scalar grid function T the system

$$L\mathbf{W} = D^{\otimes}MT$$

has to be solved, so the gradient has global stencil. The described method is exact on piecewise linear solutions, otherwise it is second order accurate in space.

Now in heat equation $aT_t - \operatorname{div}\kappa \operatorname{grad} T = f$ we use the same space discretization as described above for Poisson equation, i.e. the same discrete extended divergence and

generalized gradient operators D, G. We employ the implicit scheme (with explicit heat conductivity coefficient κ^n) written in flux form

$$a\frac{T^{n+1}-T^n}{\Delta t} + D\mathbf{W}^{n+1} = F^{n+1}$$
$$\mathbf{W}^{n+1} - GT^{n+1} = 0.$$

If we express $T^{n+1} = T^n + \Delta t/a(F^{n+1} - D\mathbf{W}^{n+1})$ and substitute it into flux equation we get

$$\mathbf{W}^{n+1} - GT^n - \Delta t/aGF^{n+1} + \Delta t/aGD\mathbf{W}^{n+1} = 0,$$

from which we can separate $\mathbf{W}^{n+1}$

$$(I + \Delta t/aGD)\mathbf{W}^{n+1} = GT^n + \Delta t/aGF^{n+1}.$$

When we apply the operator L to this equation we obtain

$$(L + \Delta t/aLGD)\mathbf{W}^{n+1} = LG(T^n + \Delta t/aF^{n+1})$$

and as $LG = LD^* = D^{\otimes}M$ the final system for $\mathbf{W}^{n+1}$ is

$$(L + \Delta t/aD^{\otimes}MD)\mathbf{W}^{n+1} = D^{\otimes}M(T^n + \Delta t/aF^{n+1}).$$

This system has local stencil and the matrix of the operator $L+\Delta t/aD^{\otimes}MD$ is symmetric and positive definite ($a = \rho\epsilon_T > 0$) so that the conjugate gradient method can be applied to iterative solution of this system. Finally having fluxes $\mathbf{W}^{n+1}$ the temperature T^{n+1} is given by

$$T^{n+1} = T^n + \Delta t/a(F^{n+1} - D\mathbf{W}^{n+1}).$$

The presented numerical method for heat equation works well on bad quality meshes appearing in Lagrangian simulations, it allows discontinuous diffusion coefficient and treats well non-linear heat waves.

6. Laser absorption. For laser absorption we employ the simplest model. The laser beam is coming from right and penetrates the material till the critical density

$$\rho_c = 1.86 \cdot 10^{-3}\frac{A}{Z\lambda_\mu^2}$$

where A is atomic number, Z plasma ionization and λ_μ laser wavelength in μm. The laser is absorbed on the critical surface which is the surface with critical density.

On the right boundary the incoming laser intensity is $\mathbf{I} = (-I(t,y), 0)$ with typically Gaussian dependence in both t and y. The (x,y) components of laser intensity are projected on the normals to the edge in the center of each edge as either $I\xi_{i,j+1/2}$ or $I\eta_{i+1/2,j}$ as shown in FIG. 6.1(a). As we need critical surface to move smoothly during simulation we use a special treatment to get values of laser intensity at each edge. The density at nodes ρ_{ij} is obtained by interpolation (weighted by subzonal volumes) from two neighboring cells on right $\rho_{i+1/2,j+1/2}$ and $\rho_{i+1/2,j-1/2}$. If both these densities are subcritical the laser penetrates to the node i,j and thus density ρ_{ij} should be also subcritical. Typically density on left of critical surface are very high (compared to critical density) and if we would interpolate density from four surrounding cells we would obtain wrong (too high)

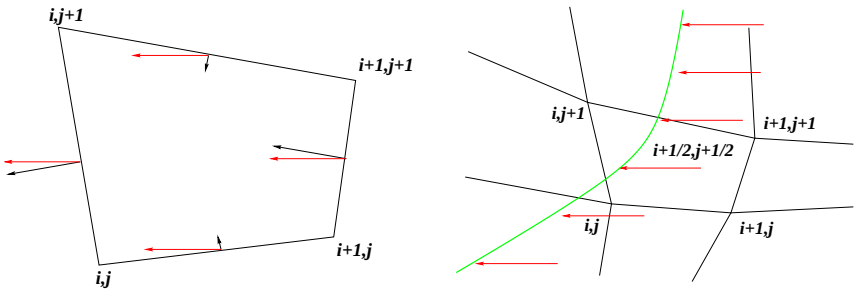

FIG. 6.1. *(a) Local projection of laser intensity to normals of edges. (b) Laser penetrates till the critical surface.*

density at nodes which are close to critical surface. Having density values in each node we can proceed to evaluate laser intensity on each edge connecting two nodes. If the density at both nodes is subritical we set updated edge length S^L to actual length of the edge. If density at both nodes is supercritical we set projected laser intensity $\mathbf{I}$ on this edge to zero. In all other cases density at one node is subcritical and at the other node is supercritical meaning that this edge intersects the critical surface. Then we find on the edge the point with critical density ρ_c (assuming density in linear on the edge) and we set updated edge length S^L to the length of the edge segment with subcritical density.

The divergence of laser intensity at the cell ij is zero if density in all four nodes of the cell is either subcritical or supercritical. Otherwise we set divergence to

$$(D\mathbf{I})_{ij} = \frac{1}{VC_{ij}}(I\xi_{i+1,j}S\xi^L_{i+1,j} - I\xi_{ij}S\xi^L_{ij} + I\eta_{i,j+1}S\eta^L_{i,j+1} - I\eta_{ij}S\eta^L_{ij})$$

which is obtained from integral of divergence over the cell replaced by integral over cell boundary. The divergence of laser intensity is included in internal energy equation (without heat conductivity)

$$\rho\frac{d\,\epsilon}{d\,t} + p\,\mathrm{div}\,\mathbf{u} = -C_a\mathrm{div}(\mathbf{I})$$

which transfers laser energy into internal energy of plasma. The laser absorption coefficient C_a is estimated by 0.5 for first and 0.75 for third harmonics. Note that the divergence of laser intensity is non-zero only for cells which are intersected by the critical surface, see FIG. 6.1(b).

7. Laser plasma simulations. We present here one application of our developed ALE code to simulation of an experiment [10] performed at Prague PALS laser facility. Pure Lagrangian code is unable to simulate this high velocity impact problem. The initial setup of the problem is presented in FIG. 7.1(a). The Aluminum disc with $d = 11\mu$m, $r = 150\mu$m is irradiated from right by intensive laser beam pulse with energy 240 J, wavelength $\lambda = 1.315$ μm and 400 ps length. The disc is ablatively accelerated towards massive Aluminum target in the 200 μm distance. The first part of simulation covers disc acceleration by laser beam and its resulting density at time $t = 3$ns is presented in FIG. 7.1(b) and shows the disc shortly before hitting the massive target. The average disc speed at this moment is 67 km/s and average temperature is 4.7 eV. The final disc data at time $t = 3$ns are interpolated to the new computational mesh and form the initial

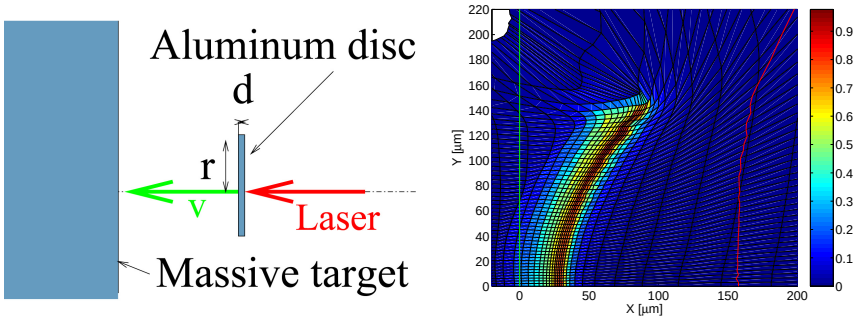

(a) (b)

FIG. 7.1. *(a) Disc flyer problem setup. (b) Density in g/cm^3 of disc flyer at $t = 3ns$, vertical blue line on left is right boundary of massive target, red curve on right is zero contour of horizontal velocity, what is left of this curve flies left what is right of this curve flies right.*

conditions to the second part of simulation which covers the high velocity impact of the disc into the massive target which creates a crater in the massive target. The temperature of the massive target at time $t = 40$ns after the impact is presented in FIG. 7.2 with three different color maps distinguishing solid (shades of gray), liquid (rainbow from blue to red) and gas (shades of brown) phases of Aluminum. Shock wave which in one part has circular shape is formed on the solid-liquid phase interface. The liquid-gas phase interface does not move further into the massive target and give us the simulated shape of crater.

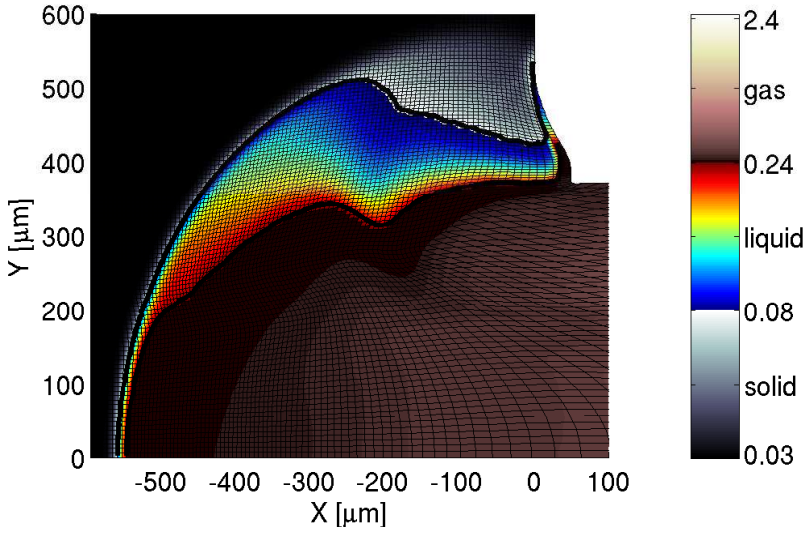

FIG. 7.2. *Temperature in eV for disc flyer problem at time $t = 40$ ns.*

Acknowledgments. The authors acknowledge the partial support of the Czech Ministry of Education grant MSM 6840770022, research center LC 528, and the Czech Grant Agency grant GACR 202/03/H162. The authors thank M. Berndt, V. Dyadechko, R. Garimella, P. Havlík, R. Loubère, L. Margolin, M. Shashkov, B. Swartz, and B. Wendroff for fruitful discussions and constructive comments.

REFERENCES

[1] R. W. Anderson, N. S. Elliott, and R. B. Pember, *An arbitrary Lagrangian-Eulerian method with adaptive mesh refinement for the solution of the Euler equations*, J. Comp. Phys., **199** (2004), 598–617.

[2] T. J. Barth, *Numerical methods for gasdynamic systems on unstructured meshes*, in An introduction to Recent Developments in Theory and Numerics for Conservation Laws, C. R. D. Kroner, M. Ohlberger, ed., Berlin, 1997, Lecture Notes in Computational Science and Engineering, Springer, 195–284.

[3] D. Benson, *Computational methods in Lagrangian and Eulerian hydrocodes*, Computer Methods in Applied Mechanics and Engineering, **99** (1992), 235–394.

[4] J. Campbell and M. Shashkov, *A tensor artificial viscosity using a mimetic finite difference algorithm*, J. Comp. Phys., **172** (2001), 739–765.

[5] J. Campbell and M. Shashkov, *A compatible Lagrangian hydrodynamics algorithm for unstructured grids*, Selcuk Journal of Applied Mathematics, **4** (2003), 53–70.

[6] E. Caramana, M. J. Shashkov, and P. Whalen, *Formulations of artificial viscosity for multi-dimensional shock wave computations*, J. Comp. Phys., **144** (1998), 70–97.

[7] E. J. Caramana, D. E. Burton, M. J. Shashkov, and P. P. Whalen, *The construction of compatible hydrodynamics algorithms utilizing conservation of total energy*, J. Comp. Phys., **146** (1998), 227–262.

[8] E. J. Caramana and M. J. Shashkov, *Elimination of artificial grid distortion and hourglass-type motions by means of Lagrangian subzonal masses and pressures*, Journal of Computational Physics, **142** (1998), 521–561.

[9] R. Garimella, M. Kuchařík, and M. Shashkov, *Efficient algorithm for local-bound-preserving remapping in ALE methods*, in Numerical Mathematics and Advanced Applications, M. Feistauer, V. Dolejsi, P. Knobloch, and K. Najzar, eds., Springer-Verlag Berlin Heidelberg New York, 2004, 358–367.

[10] S. Y. Guskov and et.al., *Investigation of shock wave loading and crater creation by means of single and double targets in pals-laser experiment*, J. of Russian Laser Research, **26** (2005), 228–244.

[11] C. W. Hirt, A. A. Amsden, and J. L. Cook, *An arbitrary Lagrangian-Eulerian computing method for all flow speeds*, J. Comp. Phys., **14** (1974), 227–253. Reprinted at *J. Comp. Phys.*, 135:203–216, 1997.

[12] P. Knupp, L. Margolin, and M. Shashkov, *Reference Jacobian optimization-based rezone strategies for arbitrary Lagrangian Eulerian methods*, J. Comp. Phys., **176** (2002), 93–128.

[13] M. Kuchařík, M. Shashkov, and B. Wendroff, *An efficient linearity-and-bound-preserving remapping method*, J. Comp. Phys., **188** (2003), 462–471.

[14] V. F. Kuropatenko, in Difference Methods for Solutions of Problems of Mathematical Physics, N. N. Janenko, ed., Amer. Math. Soc., Providence, 1967, p. 116.

[15] L. Margolin, *Introduction to "An arbitrary Lagrangian-Eulerian computing method for all flow speeds"*, J. Comp. Phys., **135** (1997), 198–202.

[16] J. S. Peery and D. E. Carroll, *Multi-material ALE methods in unstructured grids*, Comput. Methods Appl. Mech. Engrg., 187 (2000), pp. 591–619.

[17] M. Shashkov and S. Steinberg, *Solving diffusion equation with rough coefficients in rough grids*, J. Comp. Phys., **129** (1996), 383–405.

[18] M. Shashkov and B. Wendroff, *The repair paradigm and application to conservation laws*, J. Comp. Phys., **198** (2004), 265–277.

[19] L. Spitzer and R. Harm, *Transport phenomena in a completely ionized gas*, Phys. Rev., **89** (1953), 977–981.

[20] P. Váchal, R. Garimella, and M. Shashkov, *Untangling of 2D meshes in ALE simulations*, J. Comp. Phys., **196** (2004), 627–644.

[21] A. M. Winslow, *Equipotential zoning of two-dimensional meshes*, Tech. Rep. UCRL-7312, Lawrence Livermore National Laboratory, 1963.